# Receptor tyrosine phosphatase–dependent cytoskeletal remodeling by the hedgehog-responsive gene *MIM/BEG4*

Rosa Gonzalez-Quevedo, Marina Shoffer, Lily Horng, and Anthony E. Oro

Program in Epithelial Biology, School of Medicine, Stanford University, Stanford, CA 94305

During development, dynamic remodeling of the actin cytoskeleton allows the precise placement and morphology of tissues. Morphogens such as Sonic hedgehog (Shh) and local cues such as receptor protein tyrosine phosphatases (RPTPs) mediate this process, but how they regulate the cytoskeleton is poorly understood. We previously identified *Basal cell carcinoma–enriched gene 4* (*BEG4*)/*Missing in Metastasis* (*MIM*), a Shh-inducible, Wiskott-Aldrich homology 2 domain–containing protein that potentiates Gli transcription (Callahan, C.A., T. Ofstad, L. Horng, J.K. Wang, H.H. Zhen, P.A. Coulombe, and A.E. Oro. 2004. *Genes Dev.* 18:2724–2729). Here, we show that endogenous MIM is induced in a *patched1*-dependent manner and regulates the actin cytoskeleton. MIM functions by bundling F-actin, a process that requires self-association but is independent of G-actin binding. Cytoskeletal remodeling requires an activation domain distinct from sequences required for bundling in vitro. This domain associates with RPTPδ and, in turn, enhances RPTPδ membrane localization. MIM-dependent cytoskeletal changes can be inhibited using a soluble RPTPδ-D2 domain. Our data suggest that the hedgehog-responsive gene *MIM* cooperates with RPTP to induce cytoskeletal changes.

## Introduction

The organization of the actin cytoskeleton into higher order structures is an essential mechanism driving important biological functions such as changes in cell shape, adhesion, and migration (Gumbiner, 1992; Bear et al., 2001; Luo, 2002; Dent et al., 2003). During development, dynamic remodeling of the cytoskeleton allows the precise placement and orientation of developing tissues. Morphogens such as Sonic hedgehog (Shh) are global regulators that orchestrate these complex cellular behaviors to control anterior–posterior, dorsal–ventral, left–right, and proximal–distal asymmetries in metazoan organs (Meyers and Martin, 1999; Ruiz i Altaba, 1999; Gurdon and Bourillot, 2001). Increasing numbers of studies have shown that Shh is capable of directing migration and promoting cellular adhesion, although how Shh links to the cytoskeleton is unclear (Deshpande et al., 2001; Testaz et al., 2001; Charron et al., 2003; Jarov et al., 2003). Given the diversity of patterning mediated by Shh even within the same tissue, it is clear that local cues and signaling pathways are required in addition to Shh to provide context-specific morphogenetic signals. One prominent local signaling mechanism is mediated through the receptor protein tyrosine phosphatases (RPTPs). RPTPs are a large family of transmembrane proteins that contain a matrix-binding extracellular domain and a cytoplasmic tyrosine phosphatase domain (Mustelin et al., 2002; for review see Johnson and Van Vactor, 2003). RPTPs are believed to use local cues to assemble cytoplasmic signaling complexes that regulate the actin cytoskeleton, although how this is accomplished is poorly understood.

Recent work has shed light on how actin cross-linking proteins contribute to cell shape changes. The initial level of actin organization occurs through actin-nucleating proteins. These proteins assemble actin monomers into a fine meshwork of individual filaments that aid in cell shape changes (Pollard et al., 2001; Welch and Mullins, 2002). However, in vivo, actin filaments rarely exist as isolated single filaments, but instead associate into bundles or networks, in concert with actin–bundling/cross-linking proteins at key cellular sites. Numerous studies have documented the wide range in elasticity of filaments with small changes in the concentration of actin-bundling proteins (Pollard et al., 2000; Gardel et al., 2004). Similar studies have shown the need for actin-bundling proteins to achieve mechanical rigidity at the leading edge of migrating cells

Correspondence to A.E. Oro: oro@cmgm.stanford.edu

Abbreviations used in this paper: MEF, mouse embryonic fibroblast; $PIP_2$, phosphoinositol diphosphate; RPTP, receptor protein tyrosine phosphatase; Shh, Sonic hedgehog; TEM, transmission electron microscopy; WH2, Wiskott-Aldrich homology 2.

The online version of this article contains supplemental material.


The Journal of Cell Biology, Vol. 168, No. 3, January 31, 2005 453–463
http://www.jcb.org/cgi/doi/10.1083/jcb.200409078

(Xu et al., 1998; Shin et al., 2004). Loss-of-function studies demonstrate the importance of bundling proteins in processes such as cell migration, epithelial morphogenesis, and axon guidance during development (Mahajan-Miklos and Cooley, 1994; Zheng et al., 2000).

Structurally, actin-bundling proteins are modular proteins that are composed of multiple functional domains (Matsudaira, 1991; Puius et al., 1998; Revenu et al., 2004). Each consists of at least one F-actin binding domain that facilitates actin cross-linking and whose spacing and orientation determine the quality of the bundle formed. In addition to the sequences required for actin cross-linking, each protein also contains "activation" domains distinct from the bundling domain that help regulate the timing and location of bundle formation within the cell. Examples include calcium-binding domains that facilitate calcium-dependent functions (Bretscher and Weber, 1980) and protein interaction domains that allow association with microtubules or portions of the plasma membrane (Matsudaira, 1991; Stock et al., 1999; Tu et al., 2003). The existence of such a modular structure allows the rapid generation of enormous diversity in the actin cytoskeleton from a relatively small number of sequences.

In a screen for novel Shh-responsive genes, we have previously identified *Basal cell carcinoma–enriched gene 4* (*BEG4*)/*Missing in Metastasis* (*MIM*), hereafter called *MIM*, as a Shh-responsive gene in the developing hair follicle and in basal cell carcinomas of the skin (Callahan et al., 2004). MIM potentiates Gli-dependent transcription by forming complexes with the Gli transcription factor and the tumor suppressor Suppressor of Fused (Callahan et al., 2004). The previous identification of MIM binding to monomeric actin (Mattila et al., 2003; Woodings et al., 2003) suggests that MIM may be part of a growing family of cytoskeletal regulators that have effects on transcription. To help further understand the role of MIM in morphogenesis, we examined MIM function in actin cytoskeletal remodeling. Here, we show that MIM is a Shh-responsive modular protein that remodels the cytoskeleton by bundling actin filaments. We show that this activity requires self-association, F-actin binding, and an activation domain that associates with RPTPδ and is required for localizing it to the membrane. Our data suggest a mechanism by which MIM facilitates global and local cytoskeletal patterning events.

## Results

### Endogenous MIM is induced by hedgehog signaling and localizes to actin bundles

We have previously identified MIM as a Shh-responsive regulator of Gli transcription (Callahan et al., 2004). To investigate endogenous MIM protein distribution, we developed a polyclonal antibody to the first 277 amino acids of human MIM. In myc-tagged MIM-transfected 293 cell lysates, both the anti-MIM and the epitope antibody recognized the expected 110-kD band that appears as a doublet, confirming the antibody specificity (Fig. 1 A). Anti-MIM antisera, but not preimmune sera, recognized GFP-MIM–expressing cells, and this immunoreactivity could be blocked with the immunogen peptide (Fig. S1; available at http://www.jcb.org/cgi/content/full/jcb.200409078/DC1).

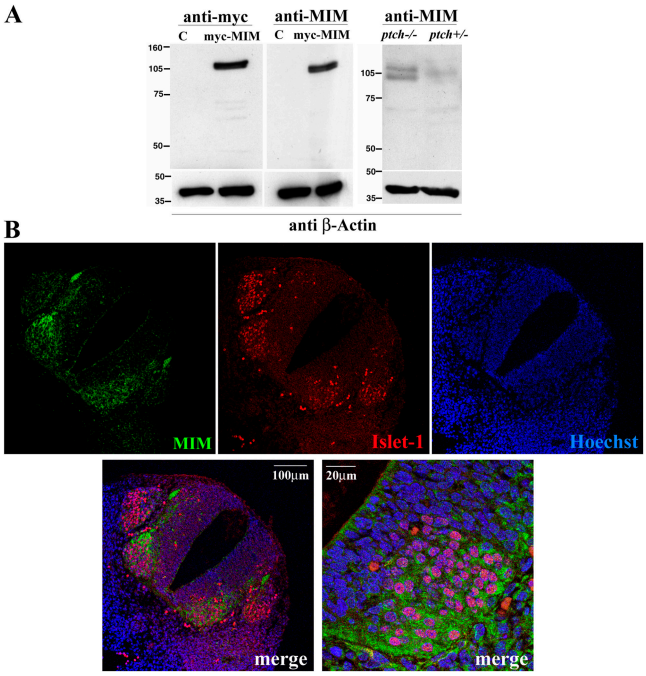


Figure 1. ***MIM is a hedgehog-responsive gene.*** (A) Characterization of the anti-MIM antibody. (left) Lysates of 293T cells untransfected (C, control) or transfected with myc-MIM and immunoblotted with an anti-myc monoclonal antibody or anti-MIM polyclonal antibody. (right) Lysates from *ptch*$^{-/-}$ and *ptch*$^{+/-}$ MEFs immunoblotted with the anti-MIM antibody. (B) MIM is expressed in a hedgehog-responsive tissue in vivo during spinal cord development. Paraffin sections of mouse neural tube at day 11.5 stained using the anti-MIM antibody. MIM (green) localizes to the Shh-responsive ventral part of the neural tube, including motor neurons (Islet-1, red). (bottom) Magnification of an area showing localization of MIM and Islet-1 to motor neurons. Nuclei (blue) are labeled with Hoechst staining.

To study MIM expression in a Shh pathway context, we used *patched (ptch)1*$^{-/-}$ mouse embryonic fibroblasts (MEFs) in which the pathway is constitutively active (Taipale et al., 2000). In *ptch1*$^{-/-}$ cells, the anti-MIM antibody recognizes two major bands, which run at 110 and 100 kD. Consistent with its role as a Shh-responsive gene, in *ptch*$^{+/-}$ MEFs in which the Shh pathway is repressed, MIM levels were dramatically reduced (Fig. 1 A, right). Similar results are seen in other *ptch1*$^{-/-}$ epithelial lines (Koike et al., 2002; unpublished data), supporting the idea that loss of *ptch1* up-regulates MIM protein expression. Shh has been shown to play an important role in the patterning of the developing neural tube as well as in axon guidance during development (Charron et al., 2003; Jacob and Briscoe, 2003; Ruiz i Altaba et al., 2003). Consequently, we attempted to determine whether MIM was expressed in this Shh-responsive tissue. Indeed, MIM immunoreactivity was detected in the cytosol of Islet-1–positive, ventral–lateral motor neurons of the neural tube (Fig. 1 B).

To characterize endogenous MIM subcellular localization, we stained *ptch1*$^{-/-}$ fibroblasts with the anti-MIM antibody. MIM accumulates on stress fibers and actin-based structures in the cytoplasm and at the membrane (Fig. 2), but decorates only a subset of stress fibers, as seen by double staining with actin (Fig. 2, A–C). In longer cytoplasmic projections,

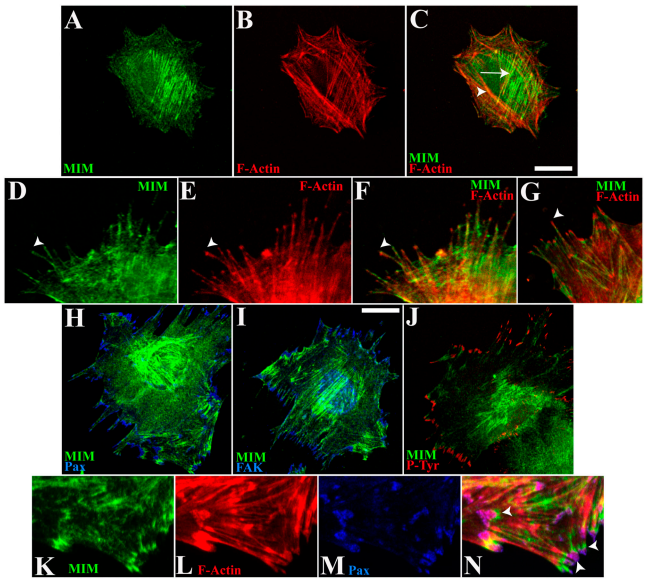


Figure 2. **Endogenous MIM localizes to actin bundles that support focal adhesion complexes.** Characterization of endogenous MIM localization in *ptch*$^{-/-}$ MEFs. (A–C) In *ptch*$^{-/-}$ cells, MIM (A, green) accumulates on a subset of stress fibers (B, red) near the center of the cell (C, arrow), but not with more peripheral cortical actin fibers (arrowhead). (D–G) MIM (D, green) decorates the length of long actin cables (E, red) at sites of membrane projections. MIM staining continues along actin bundles but is excluded from the tip of the bundle (note difference in staining near arrowheads). (H–J) MIM (green) accumulates on actin bundles that support focal adhesions complexes. Focal adhesion complexes are marked by staining with monoclonal antibodies to paxillin (H, blue), FAK (I, blue), and phosphotyrosine (J, red). (K–N) Magnified view of 2H showing that MIM (K, green) decorates the actin bundle (L, red) and is enriched in the area adjacent to paxillin-labeled focal adhesions (M, blue, and arrowheads in the merged image N). Bars, 30 μm.

MIM decorates the length of the actin bundles but is excluded from the tips of membrane projections (Fig. 2, D–G). The presence of numerous short MIM- and actin-containing structures in peripheral cell areas prompted us to try to determine whether MIM might colocalize with actin bundles at sites of focal adhesions. Consistent with this idea, double staining with markers of focal adhesion complexes such as paxillin, FAK, and phosphotyrosine epitopes confirmed that MIM is localized subjacent to focal adhesion complexes (Fig. 2, H–J). Examination of cells stained with MIM, paxillin, and F-actin demonstrated that MIM decorates actin bundles (Fig. 2 K) attached to focal adhesions (Fig. 2 L). From this data, we conclude that MIM is Shh inducible and localizes to actin bundles underlying focal adhesions.

## Cytoskeletal remodeling by MIM occurs through actin bundling

The structure and localization of MIM suggest a role in cytoskeletal remodeling. Indeed, expression of a GFP-tagged MIM in C3H10T1/2 cells induces dramatic cytoskeletal abnormalities, including loss of stress fibers, thick actin-rich structures resembling microspikes, and actin-based cell projections that are long and thicker than filopodia but narrower than lamellipodia (Fig. 3 A and Fig. S2 [available at http://www.jcb.org/cgi/content/full/jcb.200409078/DC1]). These alterations were also observed using a myc-tagged MIM in other fibroblast, epithelial, and neural cell lines, but not in cells transfected with GFP alone (Fig. 3 B; unpublished data), which supports the specificity of the effect with MIM.

Although the molecular events that generate the actin-based cell projections are complex, both actin nucleation into filaments and actin filament bundling have been shown to contribute to cell morphologic changes in vitro and in vivo (Pollard et al., 2001; Svitkina et al., 2003; Revenu et al., 2004). To determine how MIM contributes to actin remodeling, we generated a series of mutants and performed functional analysis in C3H10T1/2 cells (Fig. 3 C). We first focused on the Wiskott-Aldrich homology 2 (WH2) domain, because it had been previously implicated in MIM-induced cytoskeletal changes (Mattila et al., 2003). We confirmed previous results (Mattila et al., 2003; Woodings et al., 2003) indicating that MIM binds G-actin with high affinity ($K_d$ = 0.4 μM; Fig. 4 A). Although mutations that substitute (I735A and LK741AH) or delete (ΔWH2) conserved residues of the WH2 domain completely abrogate monomer actin binding (Fig. 4 A, lanes 10–15), the MIMΔWH2 mutant, as well as wild-type MIM, induces cytoskeletal alterations (Fig. 3, D and E). This demonstrates that the G-actin binding domain is dispensable for the observed cytoskeletal remodeling. Further evidence comes from the observation that an $NH_2$-terminal deletion mutant containing the WH2 domain (MIMΔN399) fails to induce a cytoskeletal phenotype and shows uniform cytoplasmic distribution (Fig. 3, D and E). Our data show that MIM reorganizes the actin cytoskeleton independently of its G-actin binding activity and that domains apart from the WH2 are required for cytoskeletal remodeling.

Because of the dispensability of the WH2 domain in remodeling the actin cytoskeleton, we next examined the ability of MIM to interact with F-actin. F-actin high-speed coprecipitation assays using purified GST-MIM demonstrated strong actin filament binding (Fig. 4 B, lanes 9–12), whereas the GST and BSA controls showed no significant binding (Fig. 4 B, lanes 1–4 and 17–20). The apparent binding affinity for F-actin ($K_d$ = 0.15 μM) is similar to that cited in published reports for other F-actin binding proteins (Martinez-Quiles et al., 2001). Consistent with the ability to cause a cytoskeletal phenotype, MIMΔWH2 also coprecipitated with F-actin (Fig. 4 B, lanes 13–16).

Actin filament binding of MIM in the absence of the WH2 domain led us to attempt to determine whether F-actin bundling, an activity seen in other actin-associated proteins (Loomis et al., 2003), could explain the cellular phenotype. Initially, in a low-speed F-actin cosedimentation assay, purified GST-MIM markedly induced actin filament pelleting (Fig. 4 C, lanes 3–6) compared with actin filaments alone (Fig. 4 C, lanes 1 and 2), GST control (Fig. 4 C, lanes 19–22), or in the presence of MIM mutants (Fig. 4 C, lanes 7–18). Although MIMΔWH2 pelleted actin efficiently, MIMN277 and MIMΔN399 displayed markedly reduced bundling activity in this study. We also found that MIM-dependent actin bundling was inhibited by phosphoinositol diphosphate ($PIP_2$), a hallmark of other actin cross-linking proteins (Stock et al., 1999; Fig. 4 D). Finally, we directly visualized by transmission electron microscopy (TEM) the ultrastructure of the actin

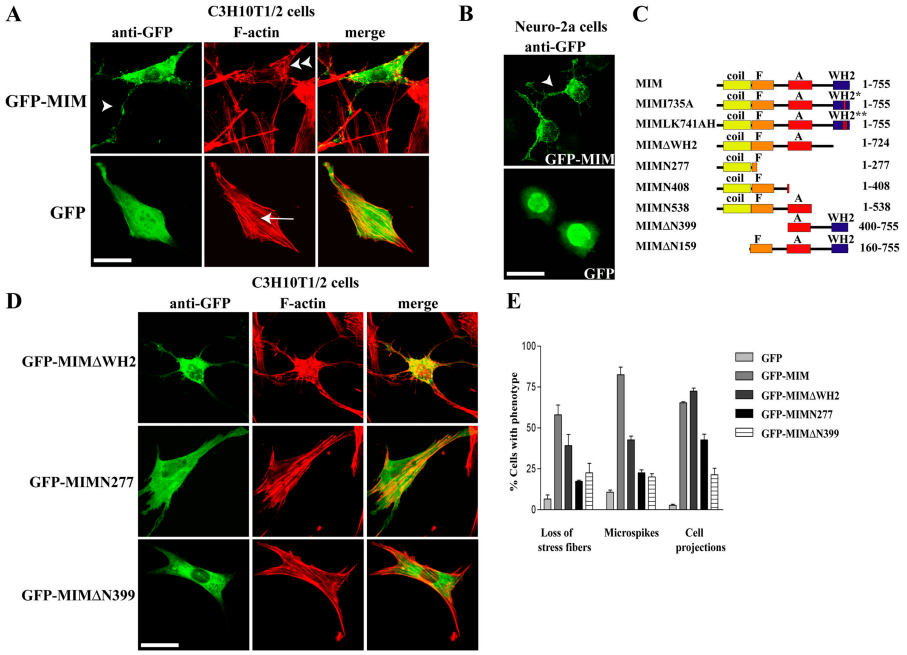


Figure 3. **MIM induces cytoskeletal changes independently of the WH2 domain.** Cytoskeletal remodeling activity of wild-type and mutant MIM proteins expressed in C3H10T1/2 cells. Cells were labeled with an anti-GFP Alexa Fluor 488 antibody (green) or phalloidin-TRITC (red, F-actin) and imaged by confocal microscopy. (A) Full-length GFP-MIM (top) or GFP (bottom). MIM induces loss of stress fibers, microspikes (double arrowhead), and actin-based cell projections (arrowhead). GFP control does not alter the cytoskeleton, and control-treated cells have well-defined stress fibers (arrow). Bar, 30 μm. (B) A similar phenotype is observed when MIM is expressed in the mouse neuroblastoma cell line Neuro-2a. The cytoskeleton is dramatically reorganized, which results in the induction of numerous cell projections (top, arrowhead), whereas the GFP control (bottom) has no effect. Bar, 35 μm. (C) Diagram of predicted domains (coil, coiled-coil; F, F-actin binding; A, activation; and WH2, WH2 domain) of MIM and the mutants used in this study. Asterisks represent the point mutations in the WH2 domain (*, substitution of I735A; **, substitution LK741,742AH). (D) The WH2 domain, but not the $NH_2$ terminus of MIM, is dispensable for the induction of cell projections. Confocal images of C3H10T1/2 cells transfected with GFP-MIMΔWH2 (1–724), GFP-MIMN277 (1–277), or GFP-MIMΔN399 (400–755). Bar, 30 μm. (E) Quantification of the phenotypes observed. Means ± SEM ($n$ = 3) are shown.

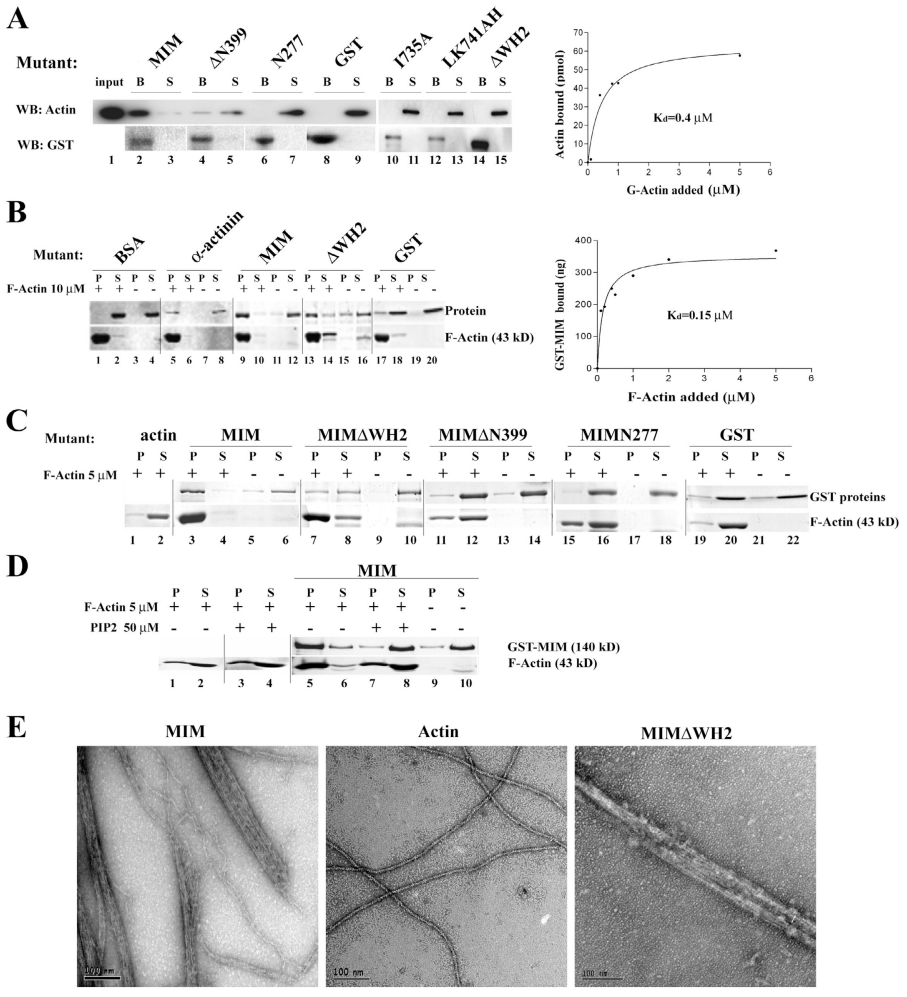


Figure 4. **MIM is a novel actin-bundling protein.** (A) The WH2 domain of MIM specifically binds G-actin. Pull-down assay from a solution of G-actin using different GST-tagged MIM proteins. Beads (B) and supernatants (S) were separated by SDS-PAGE and visualized by antiactin or anti-GST antibodies. MIM binds to monomeric actin (lanes 2 and 3), whereas substitution of critical residues (lanes 10–13) or deletion of the WH2 domain (lanes 14 and 15) completely abrogates binding. (right) Binding data determining the dissociation constant ($K_d$ = 0.4 μM) of the interaction between MIM and monomeric actin. (B) MIM binds F-actin in vitro. Purified GST-MIM proteins were incubated in the presence (+) or absence (−) of F-actin and cosedimented at 155,000 *g*. Comparative aliquots of pellet (P) and supernatant (S) were separated and gels were stained with Coomassie blue. Both MIM and MIMΔWH2 coprecipitate with F-actin (lanes 9, 10, 13, and 14). (right) Curve to establish the dissociation constant for the MIM and F-actin interaction ($K_d$ = 0.15 μM). (C) MIM cross-links actin filaments in vitro. Coprecipitation assay using purified GST-MIM proteins and F-actin at 10,000 *g*. Same aliquots of pellet (P) and supernatant (S) were separated by SDS-PAGE and stained with Coomassie blue. Apparent molecular masses of used proteins are as follows: MIM, 140 kD; MIMΔWH2, 120 kD; MIMΔN399, 75 kD; MIMN277, 50 kD; and GST, 27 kD. (D) $PIP_2$ inhibits actin bundling mediated by MIM. GST-MIM was incubated with (+) or without (−) F-actin, in the presence (+) or absence (−) of $PIP_2$. Comparable aliquots of pellet (P) and supernatant (S) were separated by SDS-PAGE and stained with Coomassie blue. In the absence of $PIP_2$, F-actin appears mostly in the pellet fraction (lanes 5 and 6), whereas in the presence of $PIP_2$, F-actin is shifted to the supernatant fraction (lanes 7 and 8). (E) Electron micrographs of actin structures in the absence or presence of equimolar amounts of 6XHis-MIM proteins, showing that MIM and MIMΔWH2 bundle actin filaments. Bars, 100 nm.

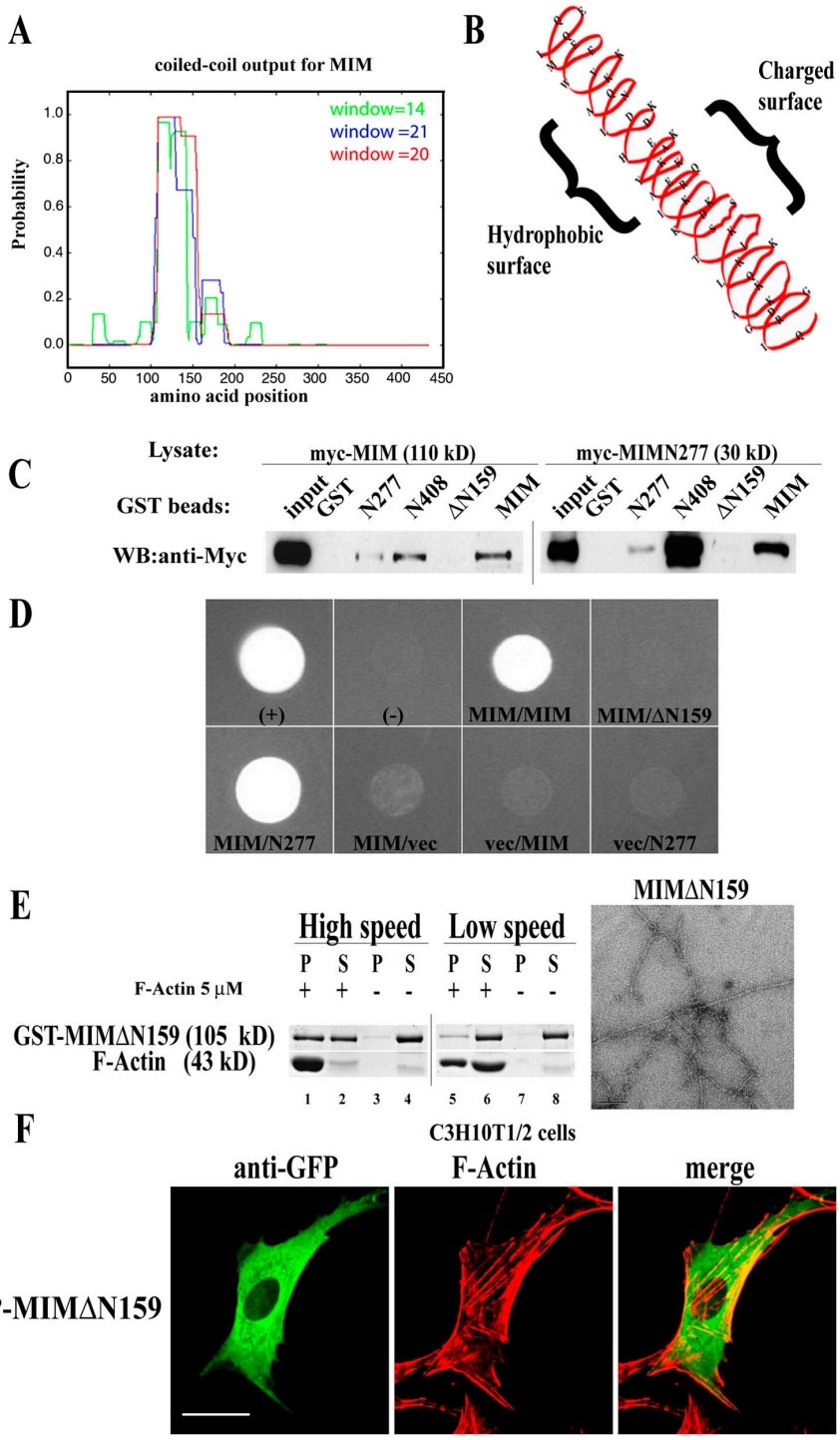


Figure 5. **MIM $NH_2$-terminal self-association domain is required for the induction of cytoskeletal changes.** (A) Diagram of the predicted coiled-coil region of MIM (http://pbil.ibcp.fr/html/pbil_index.html). (B) The coiled-coil domain is predicted to have distinct hydrophobic and hydrophilic surfaces. (C) MIM self-associates through the $NH_2$-terminal coiled-coil region. Pull-down assay from myc-MIM– or myc-MIMN277–transfected 293T cell lysates using purified GST-MIM proteins or GST bound to beads. Proteins were visualized by Western blot using an anti-myc antibody. MIM binds to GST-MIMN277 but not the control GST or MIMΔN159. (D) Yeast two-hybrid interaction assay showing single colonies from cells transformed with indicated bait/prey plasmids grown on selective media. Full-length MIM interacts with itself (MIM/MIM) or the coil domain (MIM/N277), but not with MIM lacking the coiled-coil domain (MIM/ΔN159). +, P53/Large T; −, P53/vector. MIM/vector, vector/MIM, and vector/N277 demonstrate specificity of the interaction. (E, left) Coprecipitation assay of purified GST-MIMΔN159 in the presence (+) or absence (−) of F-actin to study binding (high speed, 155,000 *g*) and bundling (low speed, 10,000 *g*). MIMΔN159 binds F-actin (lanes 1 and 2) but does not bundle (5 and 6) in vitro. (right) Electron micrographs of purified F-actin incubated with MIMΔN159. This mutant, which lacks the self-association domain, does not induce ordered bundles of filamentous actin. Bar, 100 nm. (F) Overexpression of MIMΔN159 (green) in C3H10T1/2 cells. The self-association domain is required for the induction of cytoskeletal changes. Note the presence of stress fibers (F-actin, red) and minimal cellular projections. Bar, 25 μm.

bundles induced by MIM (Fig. 4 E). Purified MIM mixed with actin filaments led to the formation of thick actin bundles. Similar bundles were seen with MIMΔWH2, which shows that MIM is sufficient to cross-link actin filaments into ordered bundles independently of the WH2 domain. Consistent with the sedimentation assays, MIMN277 and MIMΔN399 mutants demonstrated few if any of the bundles seen with full-length MIM (unpublished data). Our results from these biochemical and cell biological assays suggest that MIM bundling activity is responsible for the actin-based projections induced by MIM.

### The MIM self-association domain is required for cytoskeletal remodeling

At least two classes of actin cross-linking proteins exist, one that forms bundles through antiparallel homodimers, such as α-actinin, and another that cross-links directly through multiple F-actin binding domains on the same molecule (Matsudaira, 1991). The presence of a conserved coiled-coil domain (Fig. 5, A and B), used by actin cross-linking proteins such as the plakins (Fontao et al., 2001), suggests that MIM might fit into the former category. Based on domain analysis programs (Lupas et al., 1991), the predicted coiled-coil domain lies

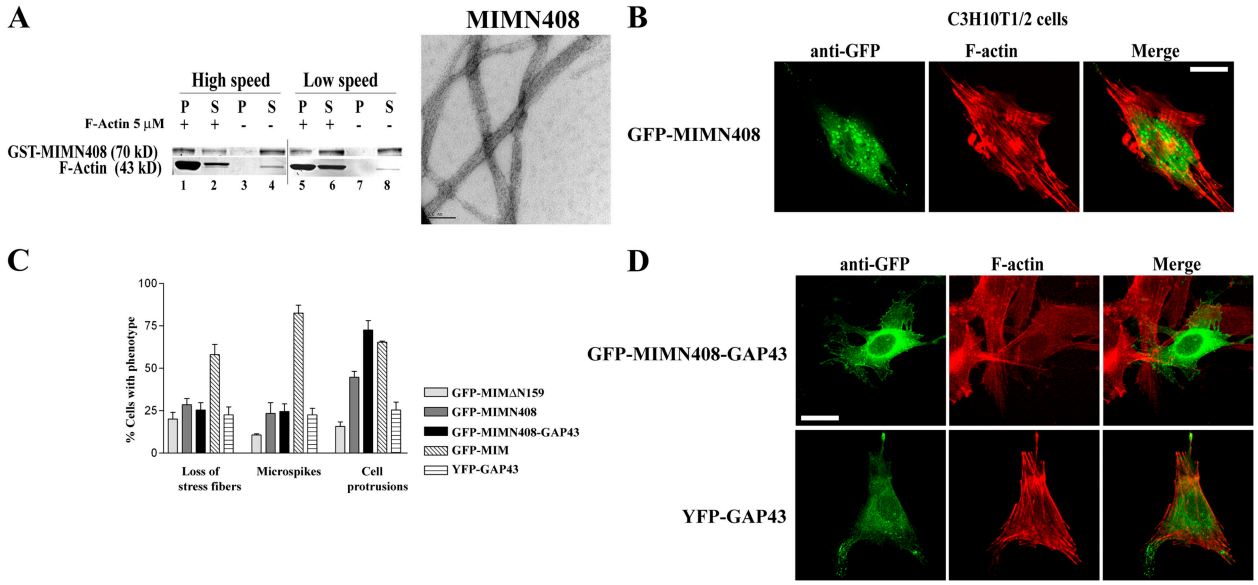


Figure 6. **Characterization of MIM membrane activation.** MIMN408 bundles actin in vitro but cannot reconstitute the phenotype of wild-type MIM in C3H10T1/2 cells. (A, left) Coprecipitation assay of purified GST-MIMN408 in the presence (+) or absence (−) of F-actin at high speed (155,000 *g*) or low speed (10,000 *g*) demonstrates both binding (lanes 1 and 2) and bundling (5 and 6). (right) Electron micrograph of MIMN408 incubated with F-actin by TEM. Bar, 100 nm. (B) Confocal microscopy of C3H10T1/2 cells expressing MIMN408. Cells show increased punctate staining in the cytosol and fewer cell projections compared with the wild type. Bar, 20 μm. (C) Quantification of phenotypes. Means ± SEM ($n$ = 3) are shown. (D) Addition of a GAP-43 tag to MIMN408 rescues the cytoskeletal phenotype. Confocal analysis of C3H10T1/2 cells expressing GFP-MIMN408-GAP43 (top, green) or control YFP-GAP43 (bottom, green). Cells were labeled with an anti-GFP antibody and F-actin (red) was visualized using phalloidin-TRITC. Bar, 25 μm.

between amino acid residues 100 and 160 and results in a surface of hydrophobic residues opposed by a surface of highly charged residues (Fig. 5 B). We examined MIM self-association using GST pull-down assays from lysates of 293T cells transfected with myc-tagged MIM constructs (Fig. 5 C). Indeed, MIM associated with itself, supporting the homodimer model. The $NH_2$-terminal fragment MIMN277 was sufficient to bind to full-length MIM, indicating that it contained the self-association domain. Moreover, MIMΔN159, a mutant lacking the coiled-coil region, failed to bind to GST-MIMN277 or wild-type MIM (Fig. 5 C). These results were confirmed genetically using a GAL4-based yeast two-hybrid interaction assay (Fig. 5 D). Cells coexpressing a MIM bait plasmid and a prey plasmid containing either MIM or MIMN277 grew on selective media, whereas cells expressing MIM plus MIMΔN159 or vector alone did not grow. These results confirm and extend previous findings (Yamagishi et al., 2004) using $NH_2$-terminal peptides and strongly argue for a specific self-association through the coiled-coil domain.

The importance of MIM self-association was further examined by testing $NH_2$-terminal mutants in F-actin binding and bundling assays (Fig. 5 E). If self-association were important for bundling, then the coiled-coil domain mutant should bind F-actin but not bundle. Consistent with this idea, MIMΔN159 bound F-actin in the high-speed coprecipitation assay, but did not bundle actin in low-speed coprecipitation and TEM analysis (Fig. 5 E). When overexpressed in C3H10T1/2 cells (Fig. 5 F), GFP-MIMΔN159 distributed uniformly throughout the cytosol and failed to induce stress fiber changes, microspikes, or cytoplasmic projections (Fig. 6 C). These data demonstrate the necessity of MIM self-association for both actin cross-linking and cellular cytoskeletal changes.

## The MIM activation domain is required for cell projection formation

Studies of other actin-bundling proteins suggest that they are modular proteins that use activation domains, polypeptides distinct from those required for actin bundling, to direct cross-linking to particular subcellular locations (Matsudaira, 1991; Puius et al., 1998). Our localization of MIM to actin bundles subjacent to focal adhesions in vivo suggests that membrane localization plays a role in activating MIM function. In our MIM structural studies we generated MIMN408, a mutant containing the first 408 amino acids of MIM that is sufficient to dimerize and bundle in vitro (Fig. 6 A). Surprisingly, this mutant shows a markedly decreased cytoskeletal phenotype with minimal microspikes, many stress fibers, and fewer cell projections (Fig. 6, B and C). Subcellular localization of MIMN408 demonstrated that it localized mainly to cytosol, puncta, and the nucleus. These data point to the existence of a putative activation domain in MIM required for proper localization/activation of bundling.

The presence of endogenous MIM in actin bundles supporting focal adhesions in *ptch*$^{-/-}$ MEFs suggests that targeting to these structures may be required for activation. To determine whether relocalization to lipid-rich areas could restore MIM activity, we fused a GAP43 membrane localization domain to the COOH terminus of MIMN408 (Fig. 6 D). The GAP43 localization domain from neuromodulin localizes proteins to cholesterol-enriched focal adhesions at the tips of cytoplasmic projections (Laux et al., 2000). Cells transfected with GFP-MIMN408-GAP43 showed increased staining on the plasma membrane and dramatically increased cell projections (Fig. 6, C and D). This mutant also increased ruffle formation, but had only

a minimal effect on stress fiber reduction or microspikes, locations not targeted by the GAP43 tag. This effect was not caused by GFP overexpression in membrane compartments, as the YFP-GAP43 control gave no detectable phenotype (Fig. 6, C and D). These data support the notion that MIM's presence at lipid-rich membrane areas is necessary, in addition to self-association and F-actin binding, for generating membrane projections.

### MIM binds to RPTPδ and relocalizes it to the membrane

To further define the components that activate MIM, we searched for candidates that associate with the MIM activation domain. The MIM COOH terminus has previously been shown to interact with RPTPδ (Woodings et al., 2003). Cell and developmental studies with RPTPδ and other Type IIa RPTPs indicate that they assemble a signaling complex at focal adhesions and are crucial in correctly organizing the cytoskeleton (for review see Johnson and Van Vactor, 2003). Initially, we examined the significance of tyrosine phosphatase activity for MIM function. We treated *ptch*$^{-/-}$ cells with the phosphatase inhibitor orthovanadate (Heffetz et al., 1990) and examined MIM localization and activity. Treated cells exhibited a dramatic reduction in MIM-associated actin cables and cytoplasmic projections (Fig. 7 A), which is consistent with a role for phosphatase activity in MIM function.

To determine whether RPTPδ binds to the MIM activation domain, we performed GST pull-down assays (Fig. 7 B). Indeed, the RPTPδ cytoplasmic domain bound strongly to full-length MIM but weakly to MIMN408 and not to the GST control (Fig. 7 B, top). This result is consistent with the reduced ability of MIMN408 to recapitulate the cell extension phenotype observed with full-length MIM. Mutants of the RPTPδ cytoplasmic tail were used to assess which portion bound to bacterially expressed MIM. Truncation mutants of RPTPδ lacking the D2 substrate binding domain did not associate with MIM, whereas D2 alone did, demonstrating that MIM binds specifically to the D2 receptor substrate binding region. These results were reproducible using bacterially expressed RPTP polypeptides (Fig. 7 B, bottom). To narrow the activation domain of MIM, we also tested binding of MIMΔN399 and MIMN538 mutants to the D2 region. Both of them showed a strong interaction with the D2 domain, suggesting that amino acids 400–538 of MIM contain the RPTPδ binding region. This latter point was further tested by expressing a GST fusion of the MIM activation domain, which showed a strong binding to the cytoplasmic domain of RPTPδ (Fig. 7 B, top).

We assayed to determine whether the RPTPδ D2–MIM interaction is required for cytoskeletal remodeling. If binding to the D2 domain at the membrane were required for MIM activity, then a soluble D2 peptide should prevent RPTP-mediated MIM membrane activation. In fact, coexpression of soluble D2 with GFP-MIM inhibited the cell extension phenotype in C3H10T1/2 cells (Fig. 7 C). This inhibition occurred in 70% of the cases. In these doubly transfected cells, MIM was distributed uniformly throughout the cytosol, similar to the ΔN159 or ΔN399 mutants. This suggests that interaction with the membrane-associated RPTP-D2 domain is required for MIM activation.

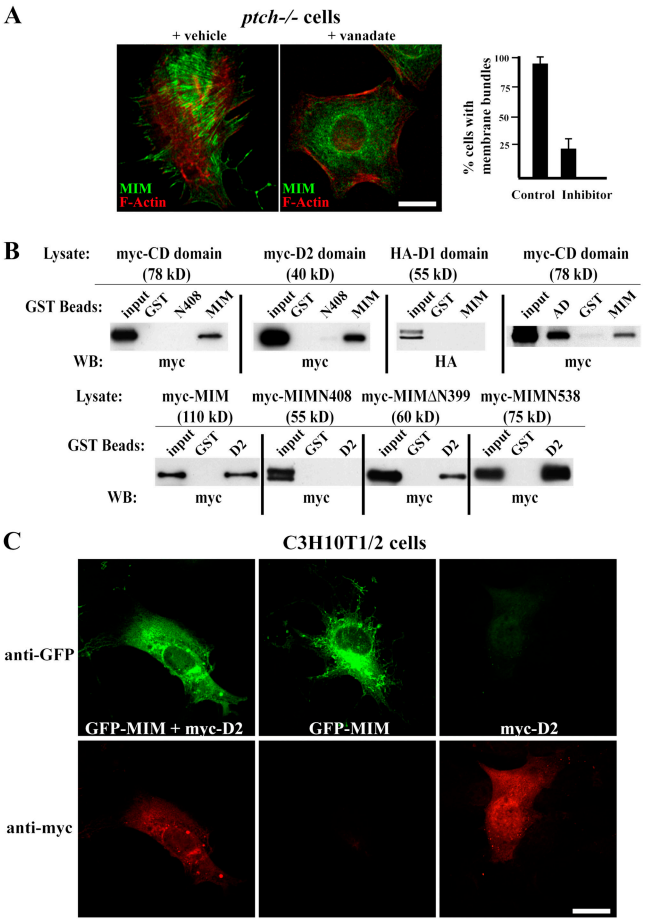


Figure 7. **MIM cytoskeletal remodeling requires interaction with the RPTPδ-D2 domain.** (A, left) Phosphatase treatment with orthovanadate (+ vanadate) inhibits endogenous MIM membrane bundles in *ptch*$^{-/-}$ cells but not in cells treated with control (+ vehicle). Confocal images of cells stained for MIM (green) and F-actin (red). Bar, 30 μm. (right) Quantification. Means ± SEM ($n$ = 3) are shown. (B) MIM amino acids 400–538 bind the substrate-binding D2 domain of RPTPδ. (top) GST pull-down assay using the indicated GST-MIM beads and cell lysates containing myc-CD (cytoplasmic domain; apparent molecular mass is 78 kD), myc-D2 (substrate binding domain 2; runs at 40 kD), or HA-D1 (catalytic domain; runs as a doublet at 55 kD). AD, MIM activation domain amino acids 401–541. (bottom) GST pull-down assay using GST-D2 or control GST beads and the indicated MIM-containing lysates. (C) Coexpression of soluble myc-D2 domain (red) with GFP-MIM (green) blocks cell projections in C3H10T1/2. Bar, 25 μm. Representative cells are shown with anti-GFP (green; top) and anti-myc (red) staining (bottom).

Although the RPTPδ–MIM interaction activates MIM-dependent cytoskeletal remodeling at the membrane, it also appears to be required for the subcellular localization of RPTPδ to the membrane. Available anti-RPTPδ antisera could detect endogenous expression by Western blot analysis but not by cell staining, so we examined RPTP distribution using transfected protein. Staining of expressed RPTPδ in the absence of MIM using a monoclonal anti-RPTPδ antibody (Pulido et al., 1995) revealed a dotlike pattern as well as cytosolic staining in C3H10T1/2 cells (Fig. 8). In the presence of MIM, the two proteins colocalized and RPTPδ distribution was dramatically enhanced at the membrane and at sites of cytoplasmic projections. MIM did not alter the localization of, or colocalize at

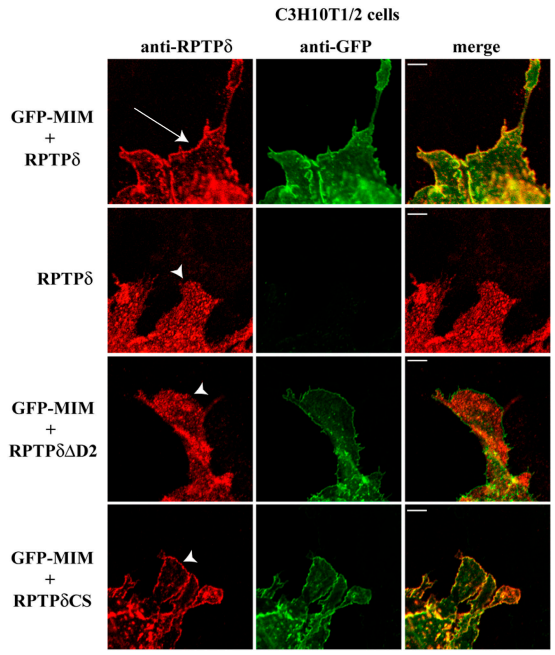


Figure 8. **MIM alters RPTPδ localization and both colocalize on the membrane.** Confocal images of C3H10T1/2 cells transfected with the indicated constructs. Cells are labeled with anti-RPTPδ antibody and anti-GFP Alexa Fluor 488. Cells coexpressing RPTPδ (red, arrow) and GFP-MIM (green) show that MIM dramatically enhances RPTPδ membrane insertion compared with cells expressing RPTP alone (arrowhead) and colocalizes with it (top two rows). (third row) MIM (green) does not colocalize or alter RPTPδ-ΔD2 distribution (red, arrowhead). (bottom) The phosphatase activity of RPTPδ is not required for the membrane relocalization as a phosphatase-dead mutant (RPTPδCS; red, arrowhead) is still inserted at the plasma membrane when coexpressed with MIM (green). Bars, 5 μm.

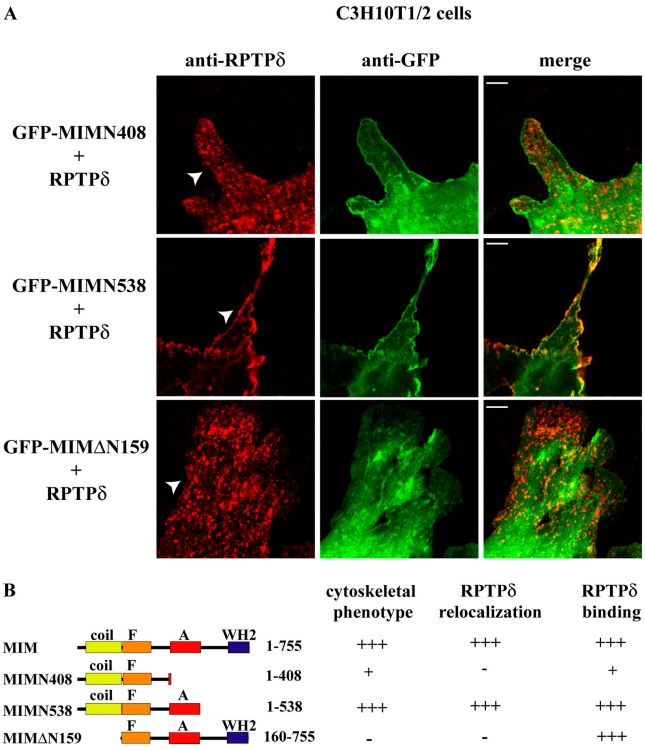


Figure 9. **MIM activation domain is required for RPTPδ membrane relocalization.** (A, top) Coexpression of GFP-MIMN408 (green) with RPTPδ (red). MIMN408 does not colocalize or affect RPTPδ distribution (top, arrowhead). However, GFP-MIMN538, a mutant that contains the activation domain, does (middle, arrowhead). (bottom) Coexpression of GFP-MIMΔN159 (green) with RPTPδ (red, arrowhead) shows that the activation domain is necessary but not sufficient for relocalizing RPTPδ, and that the bundling activity is also required. Bars, 5 μm. (B) Summary of activities of MIM and MIM mutants on the cytoskeleton and RPTPδ binding and localization.

the membrane with, RPTPδ-ΔD2, a mutant lacking the D2 domain, supporting the in vivo specificity of the interaction with RPTPδ. Because of the effects on the subcellular distribution of MIM in vanadate-treated cells, we attempted to determine whether the phosphatase activity of RPTPδ was required for its relocalization. RPTPδ containing a cysteine-to-serine mutation in the catalytic domain functioned similarly to the wild-type protein, suggesting that such activity is not required for MIM-induced relocalization.

Supporting the importance of the MIM activation domain in RPTPδ localization, MIMN408 did not relocalize nor colocalize with RPTPδ (Fig. 9). However, MIMN538, a mutant that also induces a strong cytoskeletal effect (unpublished data), showed an effect similar to that of full-length MIM (Fig. 9). In addition, MIMΔN159, the mutant that failed to self-associate and bundle (Fig. 5), did not have an effect on RPTPδ localization (Fig. 9 A, bottom), which is consistent with the idea that MIM bundling activity is required for enhanced RPTPδ membrane localization (Fig. 9 B).

## Discussion

Pattern formation during organogenesis requires precise cytoskeletal alterations in response to a variety of morphogenic stimuli. Our data show that the modular Shh effector MIM directly remodels the actin cytoskeleton by bundling actin. MIM activity is inducible and can be controlled by regulating expression via Shh signaling or by modulating activation domain interactions with RPTPδ.

The data reported here point out a crucial role for the coiled-coil domain in MIM-dependent bundling activity. In vitro, the dimerization domain aligns two actin filament binding domains to allow bundling to occur, just as it does in α-actinin and other bundling proteins. The biochemical and genetic data presented in this work with full-length MIM, in conjunction with previous biochemical data using the MIM $NH_2$ terminus (Yamagishi et al., 2004), suggest that there is a specific interaction between the MIM dimer and actin filaments, although the exact stoichiometry, affinity, and orientation of binding of the protein on the filament will require more careful biophysical studies. However, the importance of this domain is illustrated by the observation that having the activation domain without the coiled-coil domain (MIMΔN399 or MIMΔN159) is not sufficient for membrane association, strong bundling, or RPTP relocalization. This suggests that in the cell, recognition of MIM by RPTPs at the membrane requires a three-dimensional surface provided by the alignment of the dimerization domain. Interestingly, a search of GenBank sequences reveals two other proteins that have related dimerization sequences, the recently identified ABBA (Yamagishi et al., 2004) and IRSp53 (Miki et al., 2000; Nakagawa et al., 2003), which share 90% and 25% identity, re-

spectively. The similarity between MIM and these dimerization domains suggests that MIM may form heterodimers with other family members, much like members of the plakin or ezrin/radixin/moesin subfamilies of cytoskeletal regulators. Preliminary data suggest that MIM can form heterodimers (unpublished data) with ABBA, which points to additional diversity in the ability to generate cytoplasmic projections.

Our data suggest that MIM belongs to a growing family of cytoskeletal regulators that have transcriptional effects. Previously reported data indicate that MIM forms a cytoplasmic complex with Suppressor of Fused and the transcription factor Gli to regulate transcription (Callahan et al., 2004). This nuclear effect is in direct contrast to the cytoplasmic and membrane effects of actin bundling shown here. Because of recent data suggesting a role for actin binding in transcription (Olave et al., 2002), we considered the possibility that transcription was dependent on the MIM bundling domain. However, we observed that MIM potentiates transcription even without the self-association or WH2 domains that are required for actin bundling or monomeric actin binding. This supports the idea that actin bundling and transcriptional potentiation are mediated through distinct domains. Other proteins have been identified and suggested to regulate the cytoskeleton and transcription, including the Wnt pathway regulators β-catenin and plakoglobin (Moon et al., 2002; Maeda et al., 2004). Interestingly, the identification of separable domains differs from other regulators such as β-catenin that use the same domain (armadillo repeats 3–8) to bind to either adherens junctions or to TCF transcription factors (Rubinfeld et al., 1993; Su et al., 1993; Hulsken et al., 1994; Sadot et al., 1998).

Another aspect of the modular nature of MIM is the identification of distinct sequences outside the actin bundling domain that regulate bundling activity at sites of cytoplasmic projections. Colocalization studies, together with binding and cell biological experiments with a blocking polypeptide, support an important interaction domain between the RPTP D2 domain and MIM amino acids 408–538 (Figs. 7–9). RPTPs are known to assemble into large complexes of proteins that regulate the subjacent cytoskeleton during retinal and motor neuron axon pathfinding (for review see Johnson and Van Vactor, 2003). Recent data indicate that some associated proteins function to localize RPTPs to focal adhesions and neuronal synapses. For example, liprin binds to the D2 domain of another type IIa RPTP, LAR, and is required for LAR function at the synapse, in part by localizing LAR to the synapse (Serra-Pages et al., 1995, 1998; Kaufmann et al., 2002). Our data suggest a similar function for the activation domain of MIM on RPTPδ to assemble both at the membrane into specialized membrane domains. Future experiments will address whether liprin and MIM are part of the same complex and direct the RPTPs to similar or different compartments at the membrane.

The activation domain of MIM greatly enhances MIM cytoskeletal remodeling in vivo through interaction with RPTPδ. Because the cross-linking activity of many bundling proteins is activated by dephosphorylation (Zhai et al., 2001), it is tempting to speculate that MIM activity could be controlled via a competition between tyrosine phosphatases and tyrosine kinases, such as Abl or Src. This is consistent with the known association of Abl kinase with Type IIa RPTPs (Wills et al., 1999). Supporting this idea is the strong effect of phosphatase inhibitors on MIM localization and cytoskeletal activity. However, the fact that MIM408-GAP43 rescues much of the cytoskeletal phenotype by localizing MIM to focal adhesions (Fig. 6) suggests that RPTP may be playing a localizing, rather than a catalytic, role with MIM. This is supported by the ability of MIM to localize a catalytically dead RPTP to the membrane (Fig. 8) and our observation that the apparent size of MIM protein does not change in vanadate-treated cells (unpublished data). Similar results have been seen with the fly LAR protein, in which catalytically inactive LAR can rescue LAR-null animals (Krueger et al., 2003). We speculate that modification of non-RPTP accessory proteins may be required to activate MIM-dependent actin bundling activity at the membrane.

Our data provide a framework for how actin bundling proteins like MIM may coordinate effects of both global and local signaling pathways on the cytoskeleton during development. Morphogens such as Shh induce cytoskeletal regulators such as MIM and then rely on MIM's interaction with RPTPs to localize actin bundles. Interestingly, in the neural tube, MIM localizes to Shh-dependent and Islet-1–positive motor neurons, which have been shown to express RPTPδ in rats (Sommer et al., 1997). This suggests that Shh signaling and RPTP may cooperate to control motor neuron morphogenesis through MIM during spinal cord development. Future studies to examine how the activation domain of MIM regulates precise cytoskeletal changes in vivo will enhance our understanding of how morphogens such as Shh control organogenesis.

## Materials and methods

### G-actin binding assay

G-actin binding assays were performed using rabbit skeletal muscle actin (Cytoskeleton, Inc.). Actin at a final concentration of 0.05 μM (below the barbed end concentration) was incubated with 5 μg GST-MIM proteins and 20 μl of Sepharose B beads in a final volume of 100 μl. Reactions were performed in a low-salt G-actin buffer (0.2 mM $CaCl_2$, 5 mM Tris-HCl, pH 8, 0.01% $NaN_3$, and freshly added 0.2 mm ATP and 0.2 mM DTT). Western blot was performed using a monoclonal skeletal muscle actin antibody (CHEMICON International). Affinity of MIM for G-actin was determined using a G-actin binding assay and different amounts of G-actin. Blots were scanned using the GS-710 (Bio-Rad Laboratories), and densitometries of the bands were performed using the software Quantity One (Bio-Rad Laboratories). The dissociation constant was determined using the GraphPad software. Multiple experiments with different exposures gave identical affinity results.

### F-actin binding coprecipitation assays

High-speed (155,000 *g*) cosedimentation assays were performed according to the manufacturer's instructions (Cytoskeleton, Inc.). In brief, polymerized actin was incubated with GST-MIM recombinant proteins, BSA, or α-actinin. Aliquots of pellet and supernatant were run on SDS-PAGE gels and stained with Coomassie blue. For the F-actin binding curve, we incubated a fixed amount (1 μg) of purified GST-MIM with increasing amounts (0–5 μM) of polymerized actin. Fractions of inputs (F-actin added) and pellets (GST-MIM bound to F-actin) were subjected to SDS-PAGE and blotted with our purified rabbit anti-MIM antibody. Bands were quantified by densitometry. For low-speed assays, 5 μM F-actin (diluted in G buffer from 23-μM stock) was subjected to centrifugation for 1 h at RT at 10,000 *g*. After 1 h of incubation with GST-MIM recombinant proteins, samples were

spun for 1 h at 10,000 *g*. Aliquots of pellet and supernatant were run on SDS-PAGE gels and stained with Coomassie blue.

**Electron microscopy**

F-actin was polymerized as described in the previous paragraph in polymerization buffer at 23 μM and further diluted into the same buffer to 1 μM. Filaments were mixed with the recombinant proteins at ratios of 1:60 to 1:240 (actin: 6XHis-MIM proteins) and adsorbed onto glow-discharged carbon-coated copper grids for 30 s. The grid was washed with two drops of water before being stained with 1% uranyl acetate for 15 s. Electron micrographs were taken in a transmission electron microscope (model JEM-1230; JEOL) at 120 kV.

**Antibody generation**

Anti-MIM antibodies were generated by injecting purified GST-MIM amino acids 1–277 into rabbits. On day 224, sera were affinity purified over a MIM column, generated by covalently attaching purified 6XHIS-MIM 1–277 with the Amino Link kit (Pierce Chemical Co.).

**Immunocytochemistry**

C3H10T1/2, Neuro-2a, and PC12 cells were cultured as indicated by American Type Culture Collection and transfected with FuGENE (Roche). *ptch* MEFs were maintained as described previously (Taipale et al., 2000) and were serum-starved overnight before processing. Neuro-2a cells were grown on collagen 1–coated chamber slides and in 10% serum. Cells were fixed and permeabilized in 4% PFA and 1% Triton X-100 before primary antibody application. For staining of RPTPδ, cells were fixed for 10 min in 4% PFA, and then washed twice in PBS and permeabilized in 0.5% Triton X-100. Immunoreactivity was visualized with anti-GFP Alexa Fluor 488 and Alexa Fluor secondary antibodies (Molecular Bioprobes). Paxillin and FAK monoclonal antibodies (BD Biosciences), phosphotyrosine monoclonal antibody (Cell Signaling), phalloidin-TRITC (Sigma-Aldrich), anti-RPTPδ (Pulido et al., 1995), and monoclonal anti-Myc 9E10 (Sigma-Aldrich) were used as recommended by the manufacturers. Anti-MIM antibody specificity by cell staining was tested in C3H10T1/2 cells transfected with GFP-MIM and immunostained with anti-MIM antibody, preimmune serum or with the anti-MIM antibody that competed with 600 ng of immunizing peptide, followed by a secondary goat anti–rabbit Alexa Fluor 546 and Hoechst (Molecular Bioprobes) staining. For quantitation of loss of stress fibers, induction of microspikes, or cell projections, cells with projections were defined as either having three or more dendritic cell projections longer than one cell diameter or having many shorter ones with a filopodium appearance. Statistical analysis was performed using GraphPad software. Treatment of *ptch*$^{-/-}$ cells with 10 μM sodium orthovanadate was performed for 9 h. Cells were mounted in Vectashield (Vector Laboratories).

**Imaging**

Cells in Figs. 1–3 and 5–7 were visualized at RT using a confocal laser scanning system (model MRC 1024; Bio-Rad Laboratories) with a Krypton/Argon laser. Lens used was 100× oil NA 1.40 Plan Apo (Nikon). Images were acquired using Lasersharp 2000 and further processed with the Image J software. Neural tube images and Figs. 8 and 9 were collected using a confocal laser scanning microscope (model LSM 510; Carl Zeiss MicroImaging, Inc.) equipped with a Coherent Mira 900 Tunable Ti:Sapphire laser for two-photon excitation. Lasers used were Argon at 458/488/514 nm, HeNe at 543 nm, and Ti:Sapphire at 780 nm. Objectives used were Fluor 20× NA 0.75, Plan Apo 63× NA 1.40, and Plan Apo 100× oil NA 1.40. Images were acquired using the LSM 510 W.S software, version 2.5. All color images were created using Adobe Photoshop 6.0 software.

**Neural tube immunofluorescence**

Mouse embryos were collected at 11.5 d post coitum, fixed for 7 h in 4% PFA, and processed for paraffin embedding. Deparaffinized sections were blocked for 30 min in 10% sheep serum and 0.1% Tween 20, incubated for 2 h in primary antibody, and then incubated for 45 min in secondary antibody. The antibodies used were rabbit anti-MIM at 1:65 and mouse anti–Islet-1 at 1:2 (40.2D6; Developmental Studies Hybridoma Bank). The secondary antibodies used were goat anti–rabbit Alexa Fluor 488 and goat anti–mouse Alexa Fluor 546 at 1:250. The last wash included Hoechst at 1:20,000 to stain nuclei.

**Online supplemental material**

Fig. S1 shows the specificity of the anti-MIM antibody. Fig. S2 more fully characterizes the MIM-induced cytoskeletal changes in C3H10T1/2 cells. Additional methods are also included. Online supplemental material is available at http://www.jcb.org/cgi/content/full/jcb.200409078/DC1.

We thank J. Theriot, M. Footer, and J. Spudich for advice on actin biochemistry; J. Ng for technical advice; J. den Hertog, K. Johnson, and A.Tenney for constructs; M. Streuli for the RPTPδ antibody; and R. Vogelmann, M Scott, P. Khavari, and the Oro lab for helpful comments.

The work was supported by National Institutes of Health grants P01AR44012 and AR046786 (to A.E. Oro) and grants from the Secretaria de Estado de Educacion y Universidades cofunded by the European Social Fund (Ministerio de Educacion, Cultura y Deporte) and a Dean's Fellowship (to R. Gonzalez-Quevedo).

Submitted: 14 September 2004
Accepted: 17 December 2004

## References

Bear, J.E., M. Krause, and F.B. Gertler. 2001. Regulating cellular actin assembly. *Curr. Opin. Cell Biol.* 13:158–166.

Bretscher, A., and K. Weber. 1980. Villin is a major protein of the microvillus cytoskeleton which binds both G and F actin in a calcium-dependent manner. *Cell.* 20:839–847.

Callahan, C.A., T. Ofstad, L. Horng, J.K. Wang, H.H. Zhen, P.A. Coulombe, and A.E. Oro. 2004. MIM/BEG4, a Sonic hedgehog-responsive gene that potentiates Gli-dependent transcription. *Genes Dev.* 18:2724–2729.

Charron, F., E. Stein, J. Jeong, A.P. McMahon, and M. Tessier-Lavigne. 2003. The morphogen sonic hedgehog is an axonal chemoattractant that collaborates with netrin-1 in midline axon guidance. *Cell.* 113:11–23.

Dent, E.W., F. Tang, and K. Kalil. 2003. Axon guidance by growth cones and branches: common cytoskeletal and signaling mechanisms. *Neuroscientist.* 9:343–353.

Deshpande, G., L. Swanhart, P. Chiang, and P. Schedl. 2001. Hedgehog signaling in germ cell migration. *Cell.* 106:759–769.

Fontao, L., D. Geerts, I. Kuikman, J. Koster, D. Kramer, and A. Sonnenberg. 2001. The interaction of plectin with actin: evidence for cross-linking of actin filaments by dimerization of the actin-binding domain of plectin. *J. Cell Sci.* 114:2065–2076.

Gardel, M.L., J.H. Shin, F.C. MacKintosh, L. Mahadevan, P. Matsudaira, and D.A. Weitz. 2004. Elastic behavior of cross-linked and bundled actin networks. *Science.* 304:1301–1305.

Gumbiner, B.M. 1992. Epithelial morphogenesis. *Cell.* 69:385–387.

Gurdon, J.B., and P.Y. Bourillot. 2001. Morphogen gradient interpretation. *Nature.* 413:797–803.

Heffetz, D., I. Bushkin, R. Dror, and Y. Zick. 1990. The insulinomimetic agents $H_2O_2$ and vanadate stimulate protein tyrosine phosphorylation in intact cells. *J. Biol. Chem.* 265:2896–2902.

Hulsken, J., W. Birchmeier, and J. Behrens. 1994. E-cadherin and APC compete for the interaction with β-catenin and the cytoskeleton. *J. Cell Biol.* 127: 2061–2069.

Jacob, J., and J. Briscoe. 2003. Gli proteins and the control of spinal-cord patterning. *EMBO Rep.* 4:761–765.

Jarov, A., K.P. Williams, L.E. Ling, V.E. Koteliansky, J.L. Duband, and C. Fournier-Thibault. 2003. A dual role for Sonic hedgehog in regulating adhesion and differentiation of neuroepithelial cells. *Dev. Biol.* 261:520–536.

Johnson, K.G., and D. Van Vactor. 2003. Receptor protein tyrosine phosphatases in nervous system development. *Physiol. Rev.* 83:1–24.

Kaufmann, N., J. DeProto, R. Ranjan, H. Wan, and D. Van Vactor. 2002. *Drosophila* liprin-α and the receptor phosphatase Dlar control synapse morphogenesis. *Neuron.* 34:27–38.

Koike, C., T. Mizutani, T. Ito, Y. Shimizu, N. Yamamichi, T. Kameda, E. Michimukai, N. Kitamura, T. Okamoto, and H. Iba. 2002. Introduction of wild-type *patched* gene suppresses the oncogenic potential of human squamous cell carcinoma cell lines including A431. *Oncogene.* 21:2670–2678.

Krueger, N.X., R.S. Reddy, K. Johnson, J. Bateman, N. Kaufmann, D. Scalice, D. Van Vactor, and H. Saito. 2003. Functions of the ectodomain and cytoplasmic tyrosine phosphatase domains of receptor protein tyrosine phosphatase Dlar in vivo. *Mol. Cell. Biol.* 23:6909–6921.

Laux, T., K. Fukami, M. Thelen, T. Golub, D. Frey, and P. Caroni. 2000. GAP43, MARCKS, and CAP23 modulate PI(4,5)P(2) at plasmalemmal rafts, and regulate cell cortex actin dynamics through a common mechanism. *J. Cell Biol.* 149:1455–1472.

Loomis, P.A., L. Zheng, G. Sekerkova, B. Changyaleket, E. Mugnaini, and J.R. Bartles. 2003. Espin cross-links cause the elongation of microvillus-type parallel actin bundles in vivo. *J. Cell Biol.* 163:1045–1055.

Luo, L. 2002. Actin cytoskeleton regulation in neuronal morphogenesis and structural plasticity. *Annu. Rev. Cell Dev. Biol.* 18:601–635.

Lupas, A., M. Van Dyke, and J. Stock. 1991. Predicting coiled coils from protein

sequences. *Science.* 252:1162–1164.

Maeda, O., N. Usami, M. Kondo, M. Takahashi, H. Goto, K. Shimokata, K. Kusugami, and Y. Sekido. 2004. Plakoglobin (γ-catenin) has TCF/LEF family-dependent transcriptional activity in β-catenin-deficient cell line. *Oncogene.* 23:964–972.

Mahajan-Miklos, S., and L. Cooley. 1994. The villin-like protein encoded by the *Drosophila quail* gene is required for actin bundle assembly during oogenesis. *Cell.* 78:291–301.

Martinez-Quiles, N., R. Rohatgi, I.M. Anton, M. Medina, S.P. Saville, H. Miki, H. Yamaguchi, T. Takenawa, J.H. Hartwig, R.S. Geha, and N. Ramesh. 2001. WIP regulates N-WASP-mediated actin polymerization and filopodium formation. *Nat. Cell Biol.* 3:484–491.

Matsudaira, P. 1991. Modular organization of actin crosslinking proteins. *Trends Biochem. Sci.* 16:87–92.

Mattila, P.K., M. Salminen, T. Yamashiro, and P. Lappalainen. 2003. Mouse MIM, a tissue-specific regulator of cytoskeletal dynamics, interacts with ATP-actin monomers through its C-terminal WH2 domain. *J. Biol. Chem.* 278:8452–8459.

Meyers, E.N., and G.R. Martin. 1999. Differences in left-right axis pathways in mouse and chick: functions of FGF8 and SHH. *Science.* 285:403–406.

Miki, H., H. Yamaguchi, S. Suetsugu, and T. Takenawa. 2000. IRSp53 is an essential intermediate between Rac and WAVE in the regulation of membrane ruffling. *Nature.* 408:732–735.

Moon, R.T., B. Bowerman, M. Boutros, and N. Perrimon. 2002. The promise and perils of Wnt signaling through β-catenin. *Science.* 296:1644–1646.

Mustelin, T., R.T. Abraham, C.E. Rudd, A. Alonso, and J.J. Merlo. 2002. Protein tyrosine phosphorylation in T cell signaling. *Front. Biosci.* 7:d918–d969.

Nakagawa, H., H. Miki, M. Nozumi, T. Takenawa, S. Miyamoto, J. Wehland, and J.V. Small. 2003. IRSp53 is colocalised with WAVE2 at the tips of protruding lamellipodia and filopodia independently of Mena. *J. Cell Sci.* 116:2577–2583.

Olave, I.A., S.L. Reck-Peterson, and G.R. Crabtree. 2002. Nuclear actin and actin-related proteins in chromatin-remodeling. *Annu. Rev. Biochem.* 71:755–781.

Pollard, T.D., L. Blanchoin, and R.D. Mullins. 2000. Molecular mechanisms controlling actin filament dynamics in nonmuscle cells. *Annu. Rev. Biophys. Biomol. Struct.* 29:545–576.

Pollard, T.D., L. Blanchoin, and R.D. Mullins. 2001. Actin dynamics. *J. Cell Sci.* 114:3–4.

Puius, Y.A., N.M. Mahoney, and S.C. Almo. 1998. The modular structure of actin-regulatory proteins. *Curr. Opin. Cell Biol.* 10:23–34.

Pulido, R., N.X. Krueger, C. Serra-Pages, H. Saito, and M. Streuli. 1995. Molecular characterization of the human transmembrane protein-tyrosine phosphatase δ. Evidence for tissue-specific expression of alternative human transmembrane protein-tyrosine phosphatase δ isoforms. *J. Biol. Chem.* 270:6722–6728.

Revenu, C., R. Athman, S. Robine, and D. Louvard. 2004. The co-workers of actin filaments: from cell structures to signals. *Nat. Rev. Mol. Cell Biol.* 5:1–12.

Rubinfeld, B., B. Souza, I. Albert, O. Muller, S.H. Chamberlain, F.R. Masiarz, S. Munemitsu, and P. Polakis. 1993. Association of the APC gene product with beta-catenin. *Science.* 262:1731–1734.

Ruiz i Altaba, A. 1999. Gli proteins and Hedgehog signaling: development and cancer. *Trends Genet.* 15:418–25.

Ruiz i Altaba, A., V. Nguyen, and V. Palma. 2003. The emergent design of the neural tube: prepattern, SHH morphogen and GLI code. *Curr. Opin. Genet. Dev.* 13:513–21.

Sadot, E., I. Simcha, M. Shtutman, A. Ben-Ze'ev, and B. Geiger. 1998. Inhibition of β-catenin-mediated transactivation by cadherin derivatives. *Proc. Natl. Acad. Sci. USA.* 95:15339–15344.

Serra-Pages, C., N.L. Kedersha, L. Fazikas, Q. Medley, A. Debant, and M. Streuli. 1995. The LAR transmembrane protein tyrosine phosphatase and a coiled-coil LAR-interacting protein co-localize at focal adhesions. *EMBO J.* 14:2827–2838.

Serra-Pages, C., Q.G. Medley, M. Tang, A. Hart, and M. Streuli. 1998. Liprins, a family of LAR transmembrane protein-tyrosine phosphatase-interacting proteins. *J. Biol. Chem.* 273:15611–15620.

Shin, J.H., M.L. Gardel, L. Mahadevan, P. Matsudaira, and D.A. Weitz. 2004. Relating microstructure to rheology of a bundled and cross-linked F-actin network in vitro. *Proc. Natl. Acad. Sci. USA.* 101:9636–9641.

Sommer, L., M. Rao, and D.J. Anderson. 1997. RPTPδ and the novel protein tyrosine phosphatase RPTPψ are expressed in restricted regions of the developing central nervous system. *Dev. Dyn.* 208:48–61.

Stock, A., M.O. Steinmetz, P.A. Janmey, U. Aebi, G. Gerisch, R.A. Kammerer, I. Weber, and J. Faix. 1999. Domain analysis of cortexillin I: actin-bundling, PIP(2)-binding and the rescue of cytokinesis. *EMBO J.* 18:5274–5284.

Su, L.K., B. Vogelstein, and K.W. Kinzler. 1993. Association of the APC tumor suppressor protein with catenins. *Science.* 262:1734–1737.

Svitkina, T.M., E.A. Bulanova, O.Y. Chaga, D.M. Vignjevic, S. Kojima, J.M. Vasiliev, and G.G. Borisy. 2003. Mechanism of filopodia initiation by reorganization of a dendritic network. *J. Cell Biol.* 160:409–421.

Taipale, J., J.K. Chen, M.K. Cooper, B. Wang, R.K. Mann, L. Milenkovic, M.P. Scott, and P.A. Beachy. 2000. Effects of oncogenic mutations in *Smoothened* and *Patched* can be reversed by cyclopamine. *Nature.* 406:1005–1009.

Testaz, S., A. Jarov, K.P. Williams, L.E. Ling, V.E. Koteliansky, C. Fournier-Thibault, and J.L. Duband. 2001. Sonic hedgehog restricts adhesion and migration of neural crest cells independently of the Patched-Smoothened-Gli signaling pathway. *Proc. Natl. Acad. Sci. USA.* 98:12521–12526.

Tu, Y., S. Wu, X. Shi, K. Chen, and C. Wu. 2003. Migfilin and Mig-2 link focal adhesions to filamin and the actin cytoskeleton and function in cell shape modulation. *Cell.* 113:37–47.

Welch, M.D., and R.D. Mullins. 2002. Cellular control of actin nucleation. *Annu. Rev. Cell Dev. Biol.* 18:247–288.

Wills, Z., J. Bateman, C.A. Korey, A. Comer, and D. Van Vactor. 1999. The tyrosine kinase Abl and its substrate enabled collaborate with the receptor phosphatase Dlar to control motor axon guidance. *Neuron.* 22:301–312.

Woodings, J.A., S.J. Sharp, and L.M. Machesky. 2003. MIM-B, a putative metastasis suppressor protein, binds to actin and to protein tyrosine phosphatase δ. *Biochem. J.* 371:463–471.

Xu, J., D. Wirtz, and T.D. Pollard. 1998. Dynamic cross-linking by α-actinin determines the mechanical properties of actin filament networks. *J. Biol. Chem.* 273:9570–9576.

Yamagishi, A., M. Masuda, T. Ohki, H. Onishi, and N. Mochizuki. 2004. A novel actin-bundling/filopodium-forming domain conserved in insulin receptor tyrosine kinase substrate p53 and missing in metastasis protein. *J. Biol. Chem.* 279:14929–14936.

Zhai, L., P. Zhao, A. Panebra, A.L. Guerrerio, and S. Khurana. 2001. Tyrosine phosphorylation of villin regulates the organization of the actin cytoskeleton. *J. Biol. Chem.* 276:36163–36167.

Zheng, L., G. Sekerkova, K. Vranich, L.G. Tilney, E. Mugnaini, and J.R. Bartles. 2000. The deaf jerker mouse has a mutation in the gene encoding the espin actin-bundling proteins of hair cell stereocilia and lacks espins. *Cell.* 102:377–385.